Bulk and collective properties of a dilute Fermi gas in the BCS-BEC crossover

N. Manini and L. Salasnich
Dipartimento di Fisica, Università di Milano, Istituto Nazionale per la Fisica della Materia, Unità di Milano, Via Celoria 16, 20133 Milano, Italy

(Received 1 July 2004; revised manuscript received 14 October 2004; published 23 March 2005)

We investigate the zero-temperature properties of a dilute two-component Fermi gas with attractive interspecies interaction in the BCS-BEC crossover. We build an efficient parametrization of the energy per particle based on Monte Carlo data and asymptotic behavior. This parametrization provides, in turn, analytical expressions for several bulk properties of the system such as the chemical potential, the pressure, and the sound velocity. In addition, by using a time-dependent density functional approach, we determine the collective modes of the Fermi gas under harmonic confinement. The calculated collective frequencies are compared to experimental data on confined vapors of ^{6}Li atoms and with other theoretical predictions.

DOI: 10.1103/PhysRevA.71.033625 PACS number(s): 03.75.Ss, 03.75.Hh

I. INTRODUCTION

A hot topic in current many-body physics is the study of Fermi gases at ultralow temperature. Indeed, current experiments with atomic vapors are able to operate in the regime of deep Fermi degeneracy [1,2]. The two-component Fermi gases of these experiments are dilute because the effective range R_0 of the interaction is much smaller than the mean interparticle distance—i.e., $k_F R_0 \ll 1$ where $k_F=(3\pi^2 n)^{1/3}$ is the Fermi wave vector and n is the gas number density. Even in this dilute regime the s-wave scattering length a can be very large: the interaction parameter $k_F a$ can be varied over a very wide range using the Feshbach resonance technique, which permits one to vary the magnitude and the sign of a. The available experimental data on ^{6}Li atoms are concentrated across the resonance, where a goes from large negative to large positive values [3,4] and where a crossover from a Bardeen-Cooper-Schrieffer (BCS) superfluid to a Bose-Einstein condensate (BEC) of molecular pairs has been predicted [5–7].

In this paper we propose a reliable analytical fitting formula for the energy per particle of a homogeneous two-component Fermi gas by analyzing the fixed-node Monte Carlo data of Astrakharchik *et al.* [8]. From this analytical formula it is straightforward to calculate several bulk properties of the system by means of standard themodynamical relations. This fitting formula enables us to calculate also the collective modes of the Fermi gas under harmonic confinement by using the hydrodynamic theory in the local-density approximation (LDA), including also a quantum pressure term. We compare our results with other theoretical predictions [9–14] and, in particular, with the experimental frequencies of the collective breathing modes [3,4].

II. BULK PROPERTIES

At zero temperature, the bulk energy per particle, $\mathcal{E}$, of a dilute Fermi gas can be written as

$$\mathcal{E}=\frac{3}{5}\epsilon_F\epsilon(x), \tag{1}$$

where $\epsilon_F=\hbar^2k_F^2/(2m)$ is the Fermi energy and $\epsilon(x)$ is a yet unknown function of the interaction parameter $x=k_Fa$. In the weakly attractive regime ($-1\ll x<0$) one expects a BCS Fermi gas of weakly bound Cooper pairs. As the superfluid gap correction is exponentially small, the function $\epsilon(x)$ should follow the Fermi-gas expansion [15]

$$\epsilon(x)=1+\frac{10}{9\pi}x+\frac{4(11-2\ln(2))}{21\pi^2}x^2+\cdots. \tag{2}$$

In the weak BEC regime ($0<x\ll 1$) one expects a weakly repulsive Bose gas of dimers. Such Bose-condensed molecules of mass $m_M=2m$ and density $n_M=n/2$ interact with a positive scattering length $a_M=0.6a$, as predicted by Petrov *et al.* [16]. In this regime, after subtraction of the molecular binding energy, the function $\epsilon(x)$ should follow the Bose-gas expansion [17]

$$\epsilon(x)=\frac{5}{18\pi}\frac{a_M}{a}x\left[1+\frac{128}{15\sqrt{6\pi^2}}\left(\frac{a_M}{a}\right)^{3/2}x^{3/2}+\cdots\right]. \tag{3}$$

In the so-called unitarity limit ($x=\pm\infty$) one expects that the energy per particle is proportional to that of a noninteracting Fermi gas [18]. The fixed-node diffusion Monte Carlo calculation of Astrakharchik *et al.* [8] finds

$$\epsilon(x=\pm\infty)=0.42\pm 0.01, \tag{4}$$

while an analogous calculaton of Carlson *et al.* [19] gave $\epsilon(x=\pm\infty)=0.44\pm 0.01$. The calculation of Astrakharchik *et al.* [8] is quite complete and gives the behavior of the energy of system across the unitarity limit. It is a standard convention to use the inverse interaction parameter $y=1/x=1/(k_Fa)$ as the independent variable. In Fig. 1 we plot the data of $\epsilon(y)$ reported by Astrakharchik *et al.* [8,20]. On the basis of the data of Carlson *et al.* [19], Bulgac and Bertsch [14] proposed the following behavior of $\epsilon(y)$ near $y=0$:

$$\epsilon(y)=\xi-\zeta\, y+\cdots, \tag{5}$$

with $\xi=0.44$ and $\zeta=1$ for both positive and negative y. The denser data of Ref. [8] suggest instead a continuous but not differentiable behavior of $\epsilon(y)$ near $y=0$—namely, with $\xi=0.42$ and $\zeta=\zeta_-=1$ in the BCS region ($y<0$) but $\zeta=\zeta_+=1/3$ in the BEC region ($y>0$). As expected, for large $|y|$,

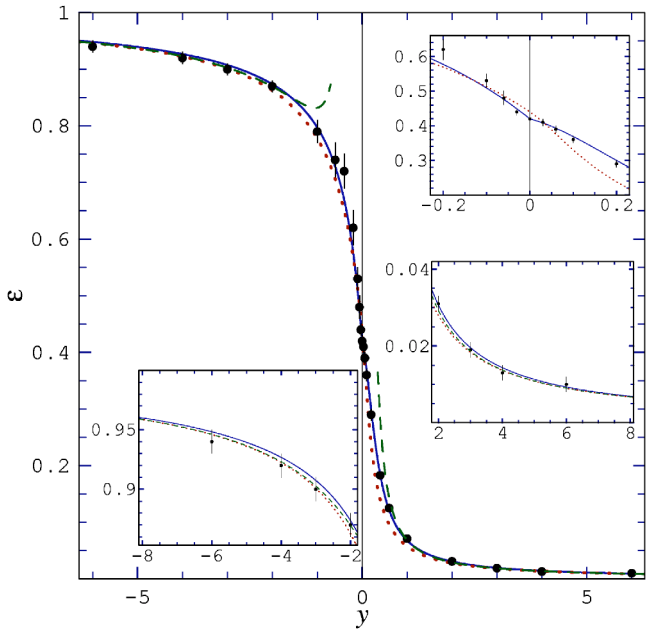

FIG. 1. The energy per particle $\epsilon(y)$ as defined in Eq. (1), where $y=1/x=1/(k_F a)$. Solid circles represent the fixed-node Monte Carlo data of Ref. [8]. The solid line is the parametric function (6) based on the values of Table I. The dotted line is the Padé approximation of Ref. [11]. Dashed lines represent the asymptotic expressions Eq. (2) and (3).

the Monte Carlo data shown in Fig. 1 follow the asymptotic trends of Eqs. (1) and (2).

We propose here the analytical fitting formula

$$\epsilon(y) = \alpha_1 - \alpha_2 \arctan\left(\alpha_3 y \frac{\beta_1 + |y|}{\beta_2 + |y|}\right), \tag{6}$$

interpolating the Monte Carlo energy per particle and the limiting behaviors for large and small $|y|$. Here the parameter α_1 is fixed by the value ξ of $\epsilon(y)$ at $y=0$, the parameter α_2 is fixed by the value of $\epsilon(y)$ at $y=\infty$, and α_3 is fixed by the asymptotic $1/y$ coefficient of $\epsilon(y)$ at large $|y|$ [Eqs. (2) and (3)]. The ratio β_1/β_2 is determined by the linear behavior ζ of $\epsilon(y)$ near $y=0$. The value of β_1 is then determined by minimizing the mean-square deviation from the Monte Carlo data [21]. Of course, we consider two different sets of parameters: one set in the BCS region ($y<0$) and a separate set in the BEC region ($y>0$). Table I reports the values of these parameters.

TABLE I. Parameters of the fitting function (6).

	BCS ($y<0$)		BEC ($y>0$)	
	Expression	Value	Expression	Value
α_1	ξ	0.4200	ξ	0.4200
α_2	$\frac{2}{\pi}(1-\alpha_1)$	0.3692	$\frac{2}{\pi}\alpha_1$	0.2674
α_3	$\frac{9\pi}{10}\alpha_2$	1.0440	$\frac{18\pi}{5}\alpha_2\frac{a_M}{a}$	5.0400
β_1	[fitted]	1.4328	[fitted]	0.1126
β_2	$\alpha_2\alpha_3\beta_1/\zeta_-$	0.5523	$\alpha_2\alpha_3\beta_1/\zeta_+$	0.4552

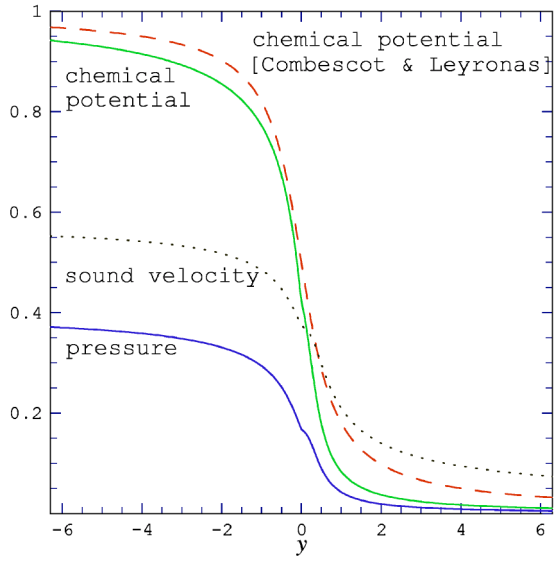

FIG. 2. Chemical potential μ/ϵ_F, pressure $P/(n\epsilon_F)$, and sound velocity c_s/v_F, obtained from the parametric function (6). The dashed line represents the simple model $\mu/\epsilon_F=\frac{1}{2}-(1/\pi)\arctan(\pi y/2)$ of Ref. [12].

Figure 1 compares this fitting function (solid curve) to the Monte Carlo data. For the sake of completeness, in Fig. 1 we also show the dotted curve obtained with the [2] Padé approximation of Kim and Zubarev [11], based only on the asymptotes and the Monte Carlo value [19] at $y=0$. Our parametric formula is more accurate, especially around $y=0$.

The advantage of a functional parametrization of $\epsilon(y)$ is that it allows straightforward analytical calculations of several ground-state physical properties of the bulk Fermi gas [22]. For example, the chemical potential μ is given by

$$\mu = \frac{\partial(n\mathcal{E})}{\partial n} = \epsilon_F\left(\epsilon(y) - \frac{y}{5}\epsilon'(y)\right), \tag{7}$$

as found by using Eq. (1) and taking into account that $\partial y/\partial n = -y/(3n)$, while the pressure P reads

$$P = n^2\frac{\partial \mathcal{E}}{\partial n} = n\epsilon_F\left(\frac{2}{5}\epsilon(y) - \frac{y}{5}\epsilon'(y)\right). \tag{8}$$

The sound velocity c_s is instead obtained as $c_s^2 = (n/m)\,\partial\mu/\partial n$, from which we get

$$c_s = v_F\sqrt{\frac{1}{3}\epsilon(y) - \frac{y}{5}\epsilon'(y) + \frac{y^2}{30}\epsilon''(y)}, \tag{9}$$

where $v_F=(2\epsilon_F/m)^{1/2}$ is the Fermi velocity. Figure 2 reports the chemical potential μ, the pressure P, and the sound velocity c_s as a function of y. Our theory predicts that all these macroscopic properties show a kink at the unitarity point, due to $\zeta_- \neq \zeta_+$. Figure 2 shows also the curve of the chemical potential obtained with the simple analytical model proposed by Combescot and Leyronas [12]. The sound velocity c_s is accessible experimentally, and the dotted curve of Fig. 2 is

our prediction of the way c_s evolves from $v_F/\sqrt{3}$ to zero through the BCS-BEC crossover.

III. HARMONICALLY CONFINED GAS

We consider now the effect of confinement due to an external anisotropic harmonic potential

$$U(\mathbf{r}) = \frac{m}{2}(\omega_\rho^2\rho^2 + \omega_z^2 z^2), \tag{10}$$

where ω_ρ is the cylindric radial frequency and ω_z is the cylindric longitudinal frequency. Assuming that the density field $n(\mathbf{r},t)$ varies sufficiently slowly (this assumption is at the basis of the LDA), at each point $\mathbf{r}$ the gas can be considered in local equilibrium and the local chemical potential is $\mu[n(\mathbf{r},t)]$. Within the LDA, the dynamics can be described by means of the hydrodynamic equations of superfluids

$$\frac{\partial n}{\partial t} + \nabla \cdot (n\mathbf{v}) = 0, \tag{11}$$

$$m\frac{\partial \mathbf{v}}{\partial t} + \nabla\left(\mu[n(\mathbf{r},t)] + U(\mathbf{r}) + \frac{1}{2}mv^2\right) = 0, \tag{12}$$

where $\mathbf{v}(\mathbf{r},t)$ is the velocity field and $\mu[n]$ is the chemical potential of Eq. (7). It has been shown by Cozzini and Stringari [23] that assuming a power-law dependence $\mu = \mu_0 n^\gamma$ for the chemical potential (polytropic equation of state [12]) from Eqs. (11) and (12) one finds analytic expressions for the collective frequencies. In particular, for the very elongated cigarshaped traps used in recent experiments ($\omega_r/\omega_z > 20$), the collective radial breathing-mode frequency Ω_ρ is given by [23]

$$\Omega_\rho = \sqrt{2(\gamma+1)}\,\omega_\rho, \tag{13}$$

while the collective longitudinal breathing-mode Ω_z is

$$\Omega_z = \sqrt{\frac{3\gamma+2}{\gamma+1}}\,\omega_z. \tag{14}$$

In our problem we introduce an effective polytropic index γ as the logarithmic derivative of the chemical potential μ—that is,

$$\gamma = \frac{n}{\mu}\frac{\partial \mu}{\partial n} = \frac{\frac{2}{3}\epsilon(y) - \frac{2y}{5}\epsilon'(y) + \frac{y^2}{15}\epsilon''(y)}{\epsilon(y) - \frac{y}{5}\epsilon'(y)}. \tag{15}$$

We have verified that indeed γ remains relatively close to unity for all y: the results of the local polytropic equation are thus useful to have a simple analytical prediction of the collective frequencies. Based on this polytropic hydrodynamic approximation (PHA), by using Eq. (6) we obtain the breathing-mode frequencies shown in Fig. 3 as dashed lines.

The analytical prediction of Eqs. (13)–(15) can be improved by releasing the polytropic approximation and explicitly integrating Eqs. (11) and (12). We have done such a calculation by including also a quantum pressure term $(-\hbar^2\nabla^2\sqrt{n})/(2m\sqrt{n})$ in Eq. (12). In practice, one must solve the following time-dependent nonlinear Schrödinger equation

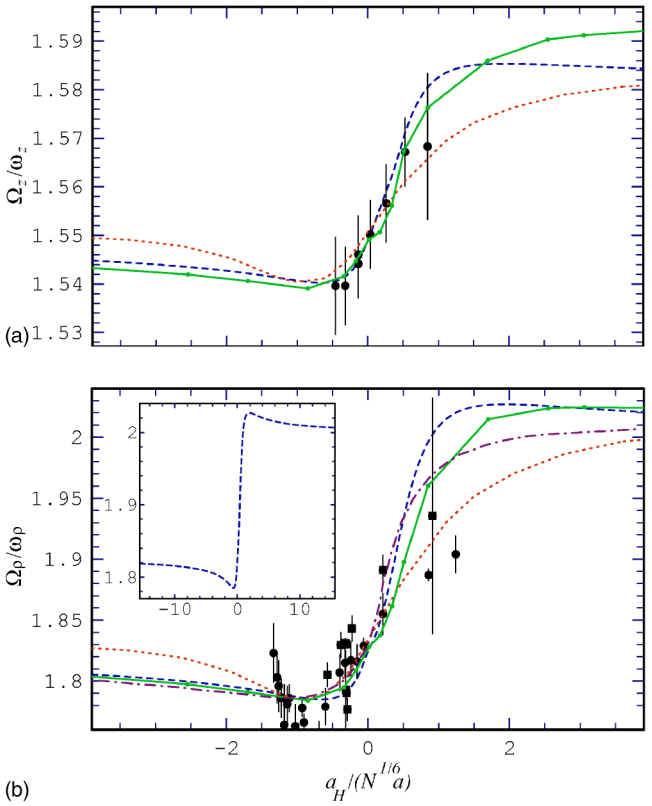

FIG. 3. Frequencies of the longitudinal and radial collective breathing modes of the Fermi gas as a function of $a_H/(N^{1/6}a) = 2^{1/2}3^{1/6}/(k_F a) = 2^{1/2}3^{1/6}y$. Ω_z experimental data from Ref. [4] and Ω_ρ experimental data from Ref. [3(a)] (squares) and Ref. [3(b)] (circles), both for ^{6}Li. Joined dots with solid lines: TDDFT of Eq. (16), with $N = 4\times10^5$, $\omega_\rho/\omega_z = 31.9$ for Ω_z and with $N = 2\times10^5$, $\omega_\rho/\omega_z = 22.1$ for ω_ρ. Dot-dashed line: variational approximation to TDDFT [11]. Dashed line: polytropic hydrodynamic approximation, Eqs. (13) and (14). Dotted line: the mean-field BCS theory of Ref. [10].

$$i\hbar\frac{\partial}{\partial t}\psi(\mathbf{r},t) = \left[-\frac{\hbar^2}{2m}\nabla^2 + U(\mathbf{r}) + \mu[n(\mathbf{r},t)]\right]\psi(\mathbf{r},t), \tag{16}$$

where $\psi(\mathbf{r},t)$ is the superfluid wave function such that $n(\mathbf{r},t) = |\psi(\mathbf{r},t)|^2$, $\mathbf{v} = \hbar\nabla\ln(\psi/n^{1/2})/(im)$, and $\mu[n]$ is the chemical potential of Eq. (7). Equation (16) can be interpreted as the Euler-Lagrange equation of a time-dependent density functional theory (TDDFT) [11]. In Ref. [11], Eq. (16) is approached via a variational scheme. Here instead, Eq. (16) is solved numerically by using a finite-difference Crank-Nicolson predictor-corrector scheme [24]. First we obtain the ground state by integrating Eq. (16) in imaginary time. Then we let a slightly perturbed wave function evolve in real time for approximately one period of oscillation of the lowest (longitudinal) frequency Ω_z. In the same time span, the density also undergoes several radial oscillations of frequency Ω_ρ. As discussed in the Appendix, we extract both frequencies by fitting the mean-square widths of $n(\mathbf{r},t)$ with the sum of two cosines. The breathing-mode frequencies ob-

tained in this way are shown in Fig. 3 as dots joined by solid lines.

The quantum pressure term is important for small number of atoms, as it improves the determination of the density profile close to the surface of the vapor cloud [11]. For the number of particles of the experiments ($N \gtrsim 10^5$), the quantum pressure term is a relatively small correction, and according to our calculation it accounts for about 0.5% of the total energy.

Figure 3 shows substantial accord between the PHA and TDDFT. The main difference is the location of the predicted maximum in the bosonic region $y>0$. The differences are not only due to the approximations involved in the PHA, but also to numerical errors in TDDFT introduced by space and time discretization (estimated to less than 1; see the Appendix). We observe that, according to our predictions, the collective frequencies reach the asymptotic large-$|y|$ limits more slowly than the theory of Hu *et al.* [10] based on mean-field BCS Bogoliubov–de Gennes equations within the LDA. In particular, in the BEC region, our numerical and analytical results (see the inset of Fig. 3) show that, contrary to the mean-field prediction, Ω_ρ approaches its asymptotic value $2\omega_\rho$ passing through a local maximum. Ω_z has the same nonmonotonic behavior while reaching $\sqrt{5/2}\omega_z$ for large y. This qualitative behavior was previously suggested by Stringari [9]. The different asymptotic behavior of the BCS mean-field frequencies is due to the neglect of beyond mean-field corrections. Note also that further discrepancies on the BEC side are due to the mean-field relation $a_m=2a_s$ rather than $a_m=0.6a_s$ as provided by four-body scattering [16] and used in our calculation. The Ω_ρ curve computed in Ref. [11] (dot-dashed line in Fig. 3) agrees rather well with our calculation.

Different theories are compared to the experimental data by Kinast *et al.* [3] for the radial mode Ω_ρ and those by Bartenstein *et al.* [4] for the longitudinal mode Ω_z. In Fig. 3, we use the standard variable $a_H/(N^{1/6}a)=2^{1/2}3^{1/6}y$ and follow Ref. [25] to determine the scattering length a as a function of the magnetic field B near the Feshbach resonance:

$$a = a_b[1 + \alpha(B - B_0)]\left[1 + \frac{\Delta}{B - B_0}\right], \qquad (17)$$

where $B_0=83.4149$ mT, $a_b=-1405\ a_0$, $\Delta=30.0$ mT, and $\alpha=0.0040(\mathrm{mT})^{-1}$. For the longitudinal frequency Ω_z, our results are in quantitative agreement with the experimental data, not unlike the mean-field prediction. The accord is less good for the radial mode. Experimental uncertainty of the position of the resonant field B_0 could partly account for these discrepancies. In particular the upward feature near $a_H/(N^{1/6}a)\simeq -1.5$ has been related [3,12] to the breaking of the Cooper pairs (due to the sizable ratio between the collective energy $\hbar\Omega_\rho$ and the gap energy Δ [12]), causing a failure of the hydrodynamical approximation. Finite-temperature and non-LDA effects not taken into account in the theories could be relevant. Note also that the experimental situation is not completely clear. The experimental measurements of Ω_ρ performed by Bartenstein *et al.* [4] (not shown in Fig. 3) disagree with the data of Kinast *et al.* [3]. In particular, Bartenstein *et al.* [4] find $\Omega_\rho/\omega_\rho \simeq 1.6$ at the unitarity limit

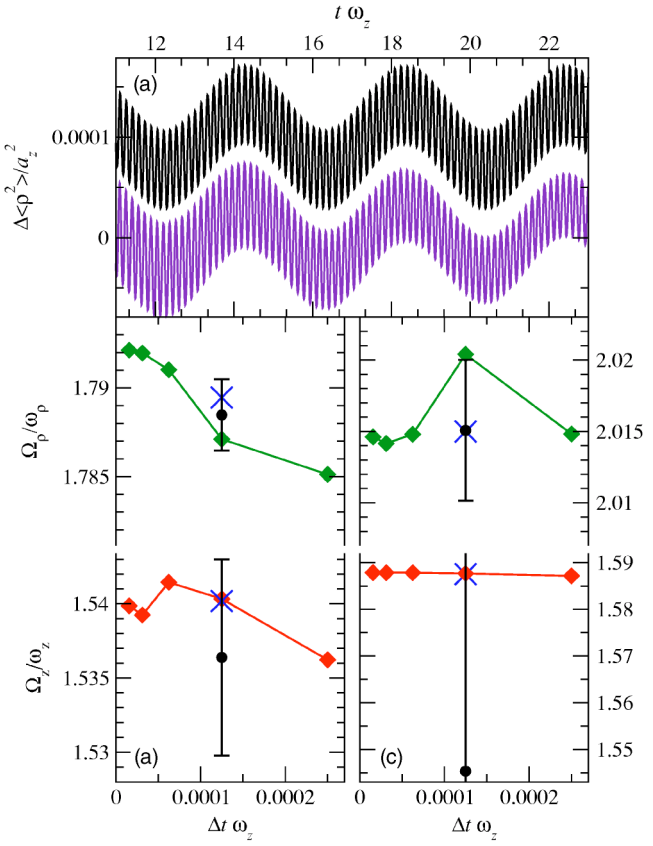

FIG. 4. Panel (a): the lower curve is the time evolution of the mean-squared radial width of the cigar-shaped Fermi gas $\Delta\langle\rho^2\rangle$ referred to its mean value; the upper curve is the fitted function $f(t)$ of Eq. (A1) displaced by 10^{-4} for clarity ($N=2\times10^5$, $\omega_\rho/\omega_z=22.1$, interaction parameter $a_H/(N^{1/6}a)=-1.69838$—i.e., $y=-1$). Panel (b): convergence of the collective breathing frequencies with the integration time interval Δt [parameters as in panel (a)], $f(t)$ fitted to an evolution time $t_{\mathrm{tot}}=4.1/\omega_z$ (diamonds), $f(t)$ fitted to an evolution time $t_{\mathrm{tot}}=41/\omega_z$(×), frequency obtained by means of Fourier transformation of the time series (circles with errorbar). Panel (c): same as panel b, but interaction parameter $a_H/(N^{1/6}a)=1.69838$—i.e., $y=1$.

$y=0$, instead of the expected value $\Omega_\rho/\omega_\rho=\sqrt{10/3}=1.82$ obtained from Eq. (13) for $\gamma=2$, characteristic of the (renormalized) free Fermi gas.

IV. DISCUSSION

We propose analytic expressions for the equations of state of a uniform dilute Fermi gas across the BCS-BEC transition. These expressions are based on recent Monte Carlo data and well-established asymptotic expansions. By using a hydrodynamic local-density approximation we include the effect of harmonic confinement. We compare the predictions of this approach with the experimental frequencies of confined ^{6}Li vapors. Other predicted physical quantites can be accessed by future experiments. The hydrodynamic approach is improved, to address small number of atoms, by including a quantum-pressure term. Indeed, our parametric formulas (6) and (7) provide an accurate expression for the μ term in Eq.

(16), which gives a better determination of the density and of the collective frequencies. This generalized quantum hydrodynamic approach, which takes into account the beyond-mean-field corrections, provides a reliable tool to determine the density profile of the fermionic cloud and to investigate its collective dynamical properties, including also mode coupling and anharmonic oscillations.

ACKNOWLEDGMENTS

The authors thank A. Parola and L. Reatto for useful discussions and J.E. Thomas for drawing their attention to new experimental determinations of Ω_ρ.

APPENDIX: NUMERICAL DETERMINATION OF THE FREQUENCIES

Figure 4(a) reports a section of a typical time evolution of the mean-square width of $n(\mathbf{r},t)$ in an asymmetric harmonic trap, computed by numerical integration of Eq. (16). The starting density is very close to the equilibrium density: it has been obtained by an initial Gaussian state evolved in imaginary time so as to filter away most of the excited components. The small residual excited components involve almost exclusively the collective breathing modes.

To extract Ω_ρ and Ω_z, one would normally resort to Fourier analysis of this time series. This approach is viable provided that the time series available is long compared to the inverse lowest frequency Ω to be determined, as the separation between adjacent Fourier frequencies is of the order of the inverse of the total integration time t_{tot}. Rather than attempting a long expensive integration of Eq. (16), we prefer to take advantage of the special character of the observed density oscillations—namely, that, as Fig. 4(a) shows, the time series contains only two characteristic frequencies (this is of course confirmed by Fourier analysis). It is therefore natural to fit the time series to the sum of two cosines:

$$f(t) = a_1\cos(\Omega_z t) + a_2\cos(\Omega_\rho t) + a_3. \tag{A1}$$

Figure 4(a) compares the computed time evolution with the fitted $f(t)$: the accord is very good, all discrepancies being related to a very weak intermode coupling. In fact, the mean-square discrepancy between the actual time evolution and the fitting function is an exceedingly sensitive function of the frequencies Ω_z and Ω_ρ: for this reason the fitting procedure must be carried out with some care, but eventually precisely this sensitivity guarantees that Ω_z and Ω_ρ are determined with high accuracy, even based on a time series shorter than the longest period of oscillation. We therefore choose this fitting method to extract the frequencies Ω_z and Ω_ρ reported as solid lines in Fig. 3 and diamonds in Figs. 4(b) and 4(c). The length of all the time series employed is $t_{\mathrm{tot}}=4.1/\omega_z$, marginally longer than one period of the Ω_z oscillation.

Figures 4(b) and 4(c) confirm the high accuracy of the method by comparing the frequency determination based on a single Ω_z period (diamond) and that based on a 10-times-longer time series ($\times$). This figure reports also the frequencies computed based on the Fourier transform of the long-time series: the accuracy of this determination of Ω_z is clearly inferior.

Figures 4(b) and 4(c) also illustrate the convergence of the computed frequency as a function of the integration time step Δt. Clearly all systematic errors induced by a finite time step and the fitting procedure are well within 1%, even with a time step $\Delta t=1.25\times10^{-4}/\omega_z$, which we adopt for all calculations of Fig. 3. The error induced by the **r**-space discretization was checked to be much smaller on the employed 200×200 cylindrical grid.

[1] M. Greiner, C. A. Regal, and D. S. Jin, Nature (London) **426**, 537 (2003).
[2] S. Jochim, M. Bartenstein, A. Altmeyer, G. Hendl, S. Riedl, C. Chin, J. Hecker Denschlag, and R. Grimm, Science **302**, 2101 (2003).
[3] (a) J. Kinast, S. L. Hemmer, M. E. Gehm, A. Turlapov, and J. E. Thomas, Phys. Rev. Lett. **92**, 150402 (2004); (b) J. Kinast, A. Turlapov, and J. E. Thomas, Phys. Rev. A **70**, 051401(R) (2004).
[4] M. Bartenstein, A. Altmeyer, S. Riedl, S. Jochim, C. Chin, J. H. Denschlag, and R. Grimm, Phys. Rev. Lett. **92**, 203201 (2004).
[5] A. J. Leggett, in *Modern Trends in the Theory of Condensed Matter*, edited by A. Pekalski and R. Przystawa (Springer, Berlin, 1980); P. Nozières and S. Schmitt-Rink, J. Low Temp. Phys. **59**, 195 (1985); J. R. Engelbrecht, M. Randeria, and C. A. R. Sa de Melo, Phys. Rev. B **55**, 15153 (1997).
[6] M. Marini, F. Pistolesi, and G. C. Strinati, Eur. Phys. J. B **1**, 151 (1998); P. Pieri and G. C. Strinati, Phys. Rev. B **61**, 15370 (2000).
[7] M. Holland, S. J. J. M. F. Kokkelmans, M. L. Chiofalo, and R. Walser, Phys. Rev. Lett. **87**, 120406 (2001); Y. Ohashi and A. Griffin, Phys. Rev. A **67**, 063612 (2003).
[8] G. E. Astrakharchik, J. Boronat, J. Casulleras, and S. Giorgini, Phys. Rev. Lett. **93**, 200404 (2004).
[9] S. Stringari, Europhys. Lett. **65**, 749 (2004).
[10] H. Hu, A. Minguzzi, X. J. Liu, and M. P. Tosi, Phys. Rev. Lett. **93**, 190403 (2004).
[11] Y. E. Kim and A. L. Zubarev Phys. Rev. A **70**, 033612 (2004).
[12] R. Combescot and X. Leyronas, Phys. Rev. Lett. **93**, 138901 (2004).
[13] H. Heiselberg, Phys. Rev. Lett. **93**, 040402 (2004).
[14] A. Bulgac and G. F. Bertsch, Phys. Rev. Lett. **94**, 070401 (2005).
[15] K. Huang and C. N. Yang, Phys. Rev. **105**, 767 (1957); T. D. Lee and C. N. Yang, *ibid.* **105**, 1119 (1957).
[16] D. S. Petrov, C. Salomon, and G. V. Shlyapnikov, Phys. Rev. Lett. **93**, 090404 (2004).
[17] T. D. Lee, K. Huang, and C. N. Yang, Phys. Rev. **106**, 1135 (1957).
[18] G. A. Baker, Jr., Phys. Rev. C **60**, 054311 (1999); Int. J. Mod. Phys. B **15**, 1314 (2001); H. Heiselberg, Phys. Rev. A **63**,

043606 (2001).
[19] J. Carlson, S.-Y. Chang, V. R. Pandharipande, and K. E. Schmidt, Phys. Rev. Lett. **91**, 050401 (2003); S.-Y. Chang, V. R. Pandharipande, J. Carlson, and K. E. Schmidt, Phys. Rev. A **70**, 043602 (2004).
[20] We thank S. Giorgini for making available to us the Monte Carlo numerical data of $\epsilon(y)$.
[21] Our parametric function has been inspired by the simpler, but much less accurate, model function proposed by Combescot and Leyronars [12].
[22] K. Huang, *Statistical Mechanics* (Wiley, New York, 1980).
[23] M. Cozzini and S. Stringari, Phys. Rev. Lett. **91**, 070401 (2003).
[24] W. H. Press, S. A. Teukolsky, W. T. Vettering, and B. P. Flannery, *Numerical Recipes in C++* (Cambridge University Press, Cambridge, England, 2002); E. Cerboneschi, R. Mannella, E. Arimondo, and L. Salasnich, Phys. Lett. A **249**, 495 (1998); L. Salasnich, A. Parola, and L. Reatto, Phys. Rev. A **64**, 023601 (2001).
[25] M. Bartenstein, A. Altmeyer, S. Riedl, R. Geursen, S. Jochim, C. Chin, J. Hecker Denschlag, R. Grimm, A. Simoni, E. Tiesinga, C. J. Williams, and P. S. Julienne, e-print cond-mat/0408673.